The Manganese Center of Oxygen-Evolving and Ca^{2+}-Depleted Photosystem II: A Pulsed EPR Spectroscopy Study

Jean-Luc Zimmermann,* Alain Boussac, and A. William Rutherford

Section de Bioénergétique (CNRS URA 1290), Département de Biologie Cellulaire et Moléculaire, Centre d'Etudes de Saclay, 91191 Gif-sur-Yvette, France

Received September 29, 1992; Revised Manuscript Received February 18, 1993

ABSTRACT: The environment of the multi-manganese center in the O_2-evolving complex (OEC) of plant photosystem II (PS II) under conditions of Ca^{2+} depletion has been probed using pulsed electron paramagnetic resonance (EPR) spectroscopy, and the following results are reported: (1) In Ca^{2+}-depleted PS II membranes treated with the chelator [ethylenebis(oxyethylenenitrilo)]tetraacetic acid (EGTA), the modified Mn EPR signal arising from the OEC in the S_2 state and the split EPR signal from the S_3 state could be detected in the absorption mode by recording the amplitude of a two-pulse echo as a function of the external magnetic field. The formation of the S_3 signal ($g \approx 2.004$; $\Delta H_{pp} = 164$ G) is not accompanied by the disappearance of the Mn EPR signal, although the signal becomes difficult to detect in CW EPR. This result supports the previous interpretation of the split S_3 EPR signal as arising from the interaction of an organic radical with the Mn cluster [Boussac, A., Zimmermann, J. L., Rutherford, A. W., & Lavergne, J. (1990) *Nature 347*, 303–306]. (2) The two-pulse electron spin echo envelope modulation (ESEEM) spectra of the S_2 state formed in Ca^{2+}-depleted PS II membranes obtained from ^{14}N- and ^{15}N-labeled material are different. This indicates that nitrogen nuclei from nitrogen-containing protein residues are coupled to the Mn center in the S_2 state of the inhibited enzyme. In addition, comparison with the two-pulse ESEEM data obtained for the S_2 state in the untreated enzyme suggests that the coupling may be altered by the Ca^{2+} depletion and/or EGTA treatment. (3) The treatment of Ca^{2+}-depleted PS II membranes with sodium pyrophosphate also induced a stable S_2 state characterized by a modified multiline EPR signal that is similar to that obtained in EGTA-treated PS II membranes. Comparison of the ESEEM data obtained for the pyrophosphate and ^{14}N and ^{15}N samples treated with EGTA suggests that the modification induced by the EGTA treatment is accompanied by the binding of (an) EGTA molecule(s) to or near the Mn center. (4) ESEEM data obtained for the S_3 state formed in the pyrophosphate or EGTA-treated enzyme are quite similar to those obtained for the corresponding S_2 state. The data are also compared with ESEEM data obtained on oxidized 4(5)-methylimidazole obtained by UV irradiation. These results are discussed with respect to the current assignment of the S_3 radical as arising from oxidation of a histidine residue.

The photosynthetic evolution of oxygen by higher plants is catalyzed by a membrane-bound protein complex called photosystem II (PS II)[1] that carries all the redox components and cofactors necessary for this reaction. The oxygen-evolving complex (OEC) contains a metal site made of four Mn ions which is probably the active site of the oxygen evolution reaction [for reviews, see Debus (1992) and Rutherford et al. (1992)]. Following successive light-induced charge separations within the reaction center of PS II, positive equivalents are sequentially transferred to and stored in the OEC, leading to $S_i \rightarrow S_{i+1}$ transitions between the five S-states (S_0–S_4) of the OEC. The S_1 state is the dark stable state, and the transient S_4 state reacts rapidly back to S_0 with the evolution of one molecule of O_2. Results from X-ray absorption spectroscopy have established that the S_1 to S_2 transition involves oxidation of one Mn ion (Yachandra et al., 1987). The nature of the oxidized species that is formed during the other S-state transitions is much less clear; however, some evidence suggests that the S_2 to S_3 transition may not correspond to a Mn oxidation: it has been proposed that an amino acid residue may become oxidized during this transition in intact PS II (Guiles et al., 1990), although recent data from X-ray absorption spectroscopy (Ono et al., 1992) seem to contradict this earlier report. In Ca^{2+}-depleted PS II, it has also been proposed that the formation of the S_3 state corresponds to the oxidation of a histidine residue (Boussac et al., 1990a).

The S_2 state of the OEC is paramagnetic, giving rise to a broad (≈1800 G) EPR multiline signal that can be detected at low temperature (Dismukes & Siderer, 1981). A recent theoretical study has shown that this EPR signal most probably arises from the magnetic exchange interaction of the four Mn ions that are present in the OEC (Bonvoisin et al., 1992). A number of treatments lead to the formation of an S_2 state that is characterized by multiline EPR signals with distinctly altered multiline patterns; these include EGTA treatment (Boussac et al., 1989) or citrate treatment (Sivaraja et al., 1989; Boussac et al., 1990b; Ono & Inoue, 1990) of Ca^{2+}-depleted PS II, the replacement of Ca^{2+} with Sr^{2+} (Boussac & Rutherford, 1988), or the treatment with NH_3 (Beck et al., 1986). Although the study of these multiline signals has produced much information regarding our knowledge of the structure and function of the OEC [for reviews, see Thorp and Brudvig (1991) and Rutherford et al. (1991, 1992)], the spectral properties of these CW EPR signals have provided limited information on the environment of the Mn center, in particular on its ligands to the protein backbone. The exact nature of the induced

* To whom correspondence should be addressed.

[1] Abbreviations: PS II, photosystem II; OEC, oxygen evolving complex; EPR, electron paramagnetic resonance or, equivalently, electron spin resonance or ESR; EDTA, (ethylenedinitrilo)tetraacetic acid; EGTA, [ethylenebis(oxyethylenenitrilo)]tetraacetic acid; CW, continuous wave; ESEEM, electron spin echo envelope modulation; ENDOR, electron nuclear double resonance; NMR, nuclear magnetic resonance; FT, Fourier transform; Im, imidazole; Tris, 2-amino-2-(hydroxymethyl)propane-1,3-diol.

0006-2960/93/0432-4831$04.00/0

modification that is characterized by the altered multiline pattern is also unclear in most cases; however, it has been demonstrated by pulsed EPR that nitrogen from ammonia couples to the Mn in NH_3-treated PS II (Britt et al., 1989).

Ca^{2+} is an essential cofactor of the oxygen evolution reaction, and a number of biochemical treatments of the OEC that cause its depletion lead to the block of the enzyme cycle after the S_3 state is formed (Boussac & Rutherford, 1988). The molecular mechanism of the interaction of Ca^{2+} with the Mn center is not known; however, when Ca^{2+} ions are removed from the OEC, an EPR signal arising from the S_3 state can be detected around $g \approx 2$, which can be assigned to a radical species that is formed during the S_2 to S_3 transition [Boussac et al., 1989, 1990a; for a review, see Debus (1992)]. When citrate, EDTA, or EGTA is present, the S_2 state gives rise to a multiline signal with a modified pattern of hyperfine lines [Boussac et al., 1989, 1990a,b; see also Sivaraja et al. (1989) and Ono and Inoue (1990)], suggesting that the close environment of the Mn complex is perturbed by the treatment. The unusual characteristics of the S_3 radical signal, in particular its relaxation properties and its split line shape, could be rationalized in a model where the organic radical with $S = {}^1/_2$ formed in the S_2 to S_3 transition interacts with the $S = {}^1/_2$ Mn complex (Boussac et al., 1990a). This radical species was proposed to be a histidine residue on the basis of its absorption spectrum in the ultraviolet (Boussac et al., 1990a). A similar EPR signal for the S_3 state has been observed in PS II inhibited by a variety of different treatments: i.e., the presence of F^- (Baumgarten et al., 1990), SO_4^{2-} (Boussac et al., 1992b), NH_3 (Andréasson & Lindberg, 1992; Hallahan et al., 1992), and acetate (McLachlan et al., 1992).

Electron spin echo envelope modulation (ESEEM) spectroscopy is a pulsed EPR method that can provide information on the small couplings from surrounding nuclei, such as protons or nitrogen atoms, to the electronic spin (Kevan, 1990). By contrast to the conventional CW EPR method, the pulsed EPR mode involves detection of the magnetization of the sample by measuring the spin echo that results from a two- or three-microwave pulse sequence. When the interpulse time between the microwave pulses is varied, the echo amplitude can be modulated by small superhyperfine couplings (ESEEM effect) that cannot be resolved in the EPR signal detected in the CW mode due to line broadenings of different sorts. Fourier analysis of the ESEEM provides frequencies that can be directly related to the nuclear transitions of the coupled nuclei (Kevan, 1990).

ESEEM results have been reported on the S_2 state of oxygen-evolving PS II prepared from spinach (Britt et al., 1989) and in ^{14}N- and ^{15}N-labeled PS II preparations isolated from the thermophilic bacterium *Synechococcus* sp. (DeRose et al., 1991). The data provided evidence for the coupling of nitrogen nuclei to the manganese center in the unperturbed S_2 state [see also Dismukes et al. (1992) for similar conclusions based on an ENDOR study]. While the existence of these small ($\approx$4–5 MHz) nitrogen couplings does not necessarily indicate nitrogen ligation to the Mn cluster, as provided, e.g., by a histidine ligand or ligands, the ESEEM data are evidence that such residues are close to the Mn complex (DeRose et al., 1991).

In this paper, we report results from pulsed EPR spectroscopy that strengthen the assignment of the S_3 signal as originating from an organic radical interacting with the Mn complex. We present ESEEM results obtained on oxygen evolving PS II that confirm earlier reports but with an increased resolution in the FT features; ESEEM data are also reported for modified charge storage states generated in the Ca^{2+}-depleted enzyme.

MATERIALS AND METHODS

Oxygen-evolving PS II membranes were prepared from market spinach as described previously (Berthold et al., 1981) with the modifications described in Boussac and Rutherford (1988). ^{15}N-labeled membranes were prepared from spinach grown on a medium supplemented with ^{15}N-labeled minerals [98% as $K^{15}NO_3$, $(^{15}NH_4)_2SO_4$, and $Ca(^{15}NO_3)$, EurisoTop, Saclay, France]. The young seedlings were collected 7 weeks after germination. The ^{15}N enrichment was estimated to be greater than 90% from the absence of the characteristic features of ^{14}N in the amide II region of the IR spectra taken on the PS II membranes (Berthomieu et al., 1992a). Ca^{2+} depletion, EGTA treatment, and reconstitution with the extrinsic polypeptides were done as described in Boussac et al. (1989). The treatment of PS II membranes with sodium pyrophosphate was analogous to the treatment with EGTA (Boussac et al., 1990b) except that 10 mM pyrophosphate replaced 10 mM EGTA [see Krieger (1992)]. Tris treatment was done as in Berthomieu et al. (1992b). Illumination of the EPR samples to advance the OEC to the S_3 state in Ca^{2+}-depleted PS II membranes was performed with an 800-W projector through IR and water filters in a nonsilvered Dewar flask containing ethanol cooled to 0 °C with liquid N_2. For illumination at 200 K of control PS II membranes, the Dewar flask contained an ethanol/solid CO_2 slush. Phenyl-*p*-benzoquinone (0.5 mM in dimethyl sulfoxide) was present as an exogenous electron acceptor in all the EPR samples except the untreated control sample. The organic radical samples were made as follows: 100 mM tyrosine, phenylalanine, tryptophan, 4(5)-CH_3-imidazole, [^{14}N]imidazole or [^{15}N]imidazole was dissolved in water with 200 mM sodium borate, and the solution was adjusted to pH 12 (or pH 10 for tyrosine). The EPR tubes were filled with the freshly prepared solutions. The EPR samples were then frozen to 77 K and illuminated in a quartz Dewar with xenon flashes ($\approx$1550 J, Quad-matic 2000 H, Bowens). Approximately 200 flashes were fired to each sample to increase the yield of the radical produced. The shape of the EPR signal produced after 200 flashes was the same as that of the signal generated by a single flash.

PS II samples suitable for both CW and pulsed EPR spectroscopies were made in quartz tubes with 3–4 mm i.d., and each sample was monitored systematically by both techniques. Complete advancement from the dark stable S_2 state to the S_3 state in Ca^{2+}-depleted PS II membranes was monitored by the complete disappearance of the multiline EPR signal and the formation of the S_3 split signal with maximal amplitude as detected by CW EPR spectroscopy in the same samples that were subsequenctly used for the pulsed EPR studies. CW EPR spectra were recorded on a Bruker ER 200D spectrometer using a standard TE_{102} cavity fitted with an Oxford Instrument liquid He cryostat. A microwave frequency counter HP 5350B and a Bruker ER035M NMR gaussmeter were used for precise measurements of the microwave frequency and the magnetic field. Pulsed EPR measurements were performed on a Bruker ER 380 pulsed EPR spectrometer equipped with a dielectric resonator, the *Q* value of which can be tuned to reduce the deadtime of the instrument due to reflection of microwaves from the resonator (ringing). Typical deadtimes of 100 ns could be achieved with the samples used in this study. The resonator was immersed in an Oxford Instrument liquid He cryostat. The

two-pulse ESEEM was measured by detecting the amplitude of the magnetization echo resulting from a $\pi/2$–τ–π microwave pulse sequence as a function of the interpulse time τ. τ was typically incremented from 112 to 6400 ns by 8-ns steps. The $\pi/2$ pulse duration was typically 8 ns with an energy of ≈300 W in the experiments reported in this study. The ESEEM data shown in this study are typically the result of 2000 accumulations. The three-pulse ESEEM was measured by detecting the amplitude of the stimulated echo resulting from a $\pi/2$–τ–$\pi/2$–T–$\pi/2$ microwave pulse sequence while incrementing the interpulse time T by steps of 8 ns and keeping τ constant. The typical microwave pulse duration was 8 or 16 ns. The value of the interpulse time τ (see legends to figures) was chosen so as to suppress the modulation (14.9 MHz at 3500 G) due to weakly coupled protons in the ESEEM (Kevan, 1990). Three-pulse ESEEM traces devoid of artifacts due to secondary echoes were obtained by using the phase cycling procedure described in Fauth et al. (1986).

For data manipulation, the data files recorded by the instrument digitizer were first transferred to a laboratory PC. A program written in C language in this laboratory was used to reformat the data under DOS. The data in the time domain were then fed into a program written in C and FORTRAN that performed the cosine-Fourier transform. The few data points missing at the beginning of the file due to deadtime were reconstructed by the Fourier backfill technique devised by Mims (1984). The program used was largely based on a data analysis program that was kindly made available to us by Prof. John McCracken (University of Michigan).

To analyze the relative differences between the ESEEM data of the S_3 and S_2 states, the ESEEM data in the time domain were divided (see legends to Figures) in a manner similar to that described by Mims et al. (1984). This procedure proved to be more efficient in characterizing the changes between the two data files than subtraction of the data from these samples.

RESULTS

Oxygen-Evolving Photosystem II. Figure 1A shows traces of the echo amplitude as a function of the magnetic field that was measured for a sample of oxygen-evolving (control) PS II membranes that were dark adapted in the S_1 state (trace a) and in the S_2 state produced by a period of illumination at 200 K (trace b). In this sample it was found that a small proportion of high-potential cytochrome b_{559} is oxidized in the dark. The two traces were scaled so that in both spectra the amplitudes of the low-field feature arising from the g_z = 3.03 component of this cytochrome exactly match. The increase in magnetization between 2500 and 4500 G that is shown in Figure 1A upon forming the S_2 state is due to the formation of the Mn S_2 EPR signal. The spectrum that is obtained after numerical differentiation of trace b *minus* trace a is shown in Figure 1A (inset): it shows a multiline pattern that is similar to the pattern displayed by the S_2 multiline EPR signal when measured in the more conventional field modulated, CW mode [a similar result was shown by Britt et al. (1989)]. This confirms that the magnetization that is measured under the conditions of Figure 1Aa largely originates from the Mn OEC in the S_2 state. We estimate from the CW EPR spectra recorded on the same samples that a maximum of 10% of cyt b_{559} is photooxidized during the illumination period. However, since the g_z feature of the cyt b_{559}^+ EPR signal does not interfere with the S_2 EPR multiline signal, the method of scaling based on the amplitude of this g_z feature will merely lead to a slight underestimate of the photoinduced

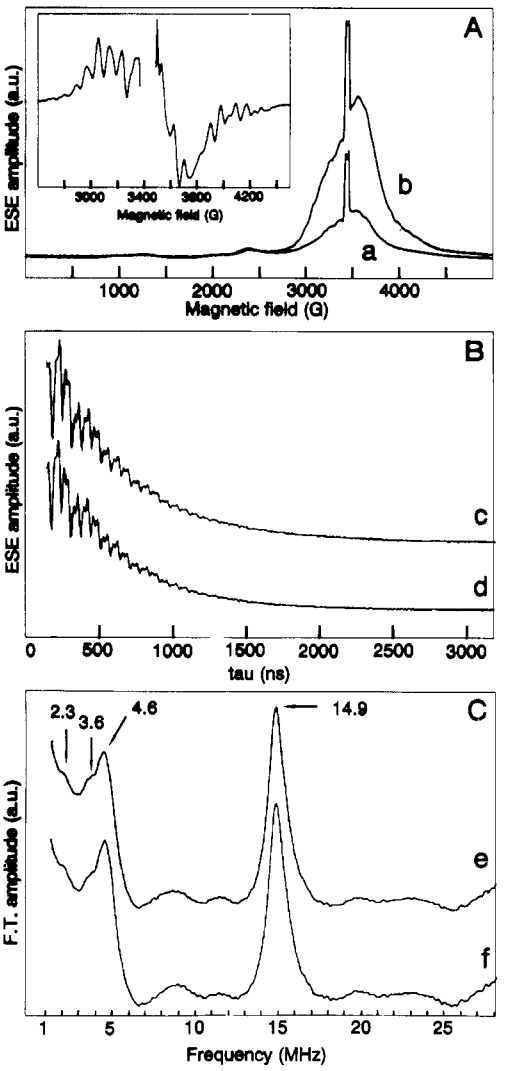

FIGURE 1: (Panel A) Amplitude of the electron spin echo resulting from a two-pulse sequence, as a function of the magnetic field. Trace a is obtained in dark-adapted PS II membranes and trace b is obtained after a 6-min illumination at 200 K; τ = 200 ns, f = 9.63 GHz, and the time interval between successive pulse sets is 1.0 ms. The inset shows the derivative with respect to the magnetic field of the spectrum resulting from subtracting trace a from trace b and displays the light-induced multiline signal. (Panels B and C) Two-pulse ESEEM data (B) and cosine-Fourier transform (C) for the sample in the S_2 state. The data were obtained at a magnetic field of 3480 G, microwave frequency of 9.64 GHz, and temperature of 4.3 K. The interpulse time s was incremented from 120 to 3312 ns in 8-ns steps. Traces c and e were obtained for the illuminated sample (raw data), while traces d and f were obtained after subtracting the ESEEM from the signal measured in the dark at 3480 G (corrected data).

S_2 EPR multiline signal. In addition, the differentiated spectrum seems to show features at around 3600 G which may arise from the g = 1.9 form of the semiquinone Fe^{2+} acceptor complex of PS II (Rutherford & Zimmermann, 1984). The significance of the possible interferences of the semiquinone Fe^{2+} and oxidized cyt b_{559} EPR signals with the Mn signal is discussed below.

The ESEEM that is measured for the sample of oxygen-evolving PS II membranes in the S_2 state at 3480 G, i.e., at a magnetic field position where the contribution of the S_2 EPR signal dominates, is shown in Figure 1Bc (raw data). Figure 1Bd also shows the ESEEM signal that is obtained after the ESEEM from the background signal measured at 3480 G (i.e., before the illumination period) was subtracted from the ESEEM trace of Figure 1Bc (corrected data). The

corresponding cosine-FT spectra are shown in Figure 1Ce for the raw data and Figure 1Cf for the corrected data. The two spectra are virtually identical, indicating very little contribution from the background ESEEM in the features shown in Figure 1C. This demonstrates that all the peaks that are resolved in the Fourier transform in Figure 1C correspond to light-induced couplings that are largely attributable to the Mn in the S_2 state and not from unspecific background signals. The spectra shown in Figure 1C resemble those obtained by Britt et al. (1989) and DeRose et al. (1991) on similar types of samples. Two main features are evident in the FT spectrum. First, a ≈0.7-MHz wide peak centered at 14.9 MHz that can be assigned to weakly coupled protons on the basis of the observations made by Britt (1988). As expected, the frequency position of this peak scales with the magnetic field when the ESEEM is measured at other field positions throughout the EPR signal (not shown). Secondly, a feature with a major peak at 4.6 MHz is evident at lower frequency with additional partially resolved features at ≈2.3 and ≈3.6 MHz. These peaks were also resolved in the FT ESEEM measured at several other magnetic fields ranging from 2900 to 4300 G (not shown). This feature is reminiscent of the broad peak observed at a similar frequency position in the ESEEM spectra of similar samples: 4.7 MHz measured by Britt et al. (1989) and 4.5 MHz by DeRose et al. (1991). Since those peaks were shown to originate from superhyperfine couplings with ^{14}N nuclei, the low-frequency feature in Figure 1C is similarly assigned to coupling(s) to ^{14}N nuclei from nitrogen-containing protein residues. The spectrum of Figure 1C shows increased resolution in the ^{14}N frequency peak compared to the spectra already reported in the literature (Britt et al., 1989; DeRose et al., 1991). It is of note that a shoulder seems to be visible on the low-frequency side of the 4.5-MHz peak shown by DeRose et al. (1992), that could correspond to some of the resolved peaks reported here [see Figure 3b in DeRose et al. (1992)].

Ca^{2+}-Depleted Photosystem II. It has been shown that when PS II membranes are depleted of Ca^{2+} ions, the S_3 state is characterized by an EPR signal centered close to $g \approx 2$ and having a derivative-like line shape (Boussac et al., 1989). Under some experimental conditions, the signal was shown to be split, and a detailed analysis of the line shape and spectral properties of this EPR signal showed that it could be simulated by the relatively weak magnetic interaction (exchange interaction $J \approx 0.01$ cm^{-1}) between a radical species and the manganese cluster with $S = {}^1/_2$ (Boussac et al., 1990a). Since the S_2 to S_3 transition involves storage of a single oxidative equivalent and since a radical is formed, it was concluded that no Mn was oxidized during this transition and that in the S_3 state the Mn cluster was in the same redox and spin states as in the S_2 state. However, the formation of the S_3 EPR signal is accompanied by the disappearance of the Mn S_2 multiline signal as detected in the CW derivative mode (Boussac et al., 1989, 1990a). The model outlined in Boussac et al. (1990a) explained the inability to detect the Mn multiline signal in the S_3 state by inhomogeneous line broadening induced by (i) the nonresolution of the extra line splitting originating from the magnetic interaction and/or (ii) the dipolar interaction between the two spin systems. If line broadening is actually the origin of the disappearance of the Mn multiline signal in the CW derivative mode, it is possible that it might be detected under conditions where direct measurement of the absorption EPR signal is made.

Figure 2Ab shows the trace of the two-pulse echo amplitude that is obtained when the magnetic field is swept for a Ca^{2+}-depleted PS II sample treated with EGTA, with the 24- and 17-kDa extrinsic polypeptides reconstituted, and adapted in the dark, i.e., in the S_2 state (Boussac et al., 1989). The feature at ≈2400 G (that was also partly present in Figure 1A) is assigned to the g_z feature of cyt b_{559} that is largely oxidized under these conditions (Boussac et al., 1989). The broad signal that culminates at about 3350 G and extends over at least 1500 G is assigned to the S_2 EPR signal. Other points pertinent to this assignment are given below. It is worth noting that the modified multiline pattern that is characteristic of the signal measured in the CW mode is very difficult to detect in this measurement (see Figure 3c), presumably due to the smaller line spacing of the Mn multiline pattern and to the lower amplitudes of the hyperfine lines. Figure 2Aa shows the spectrum obtained under the same conditions for

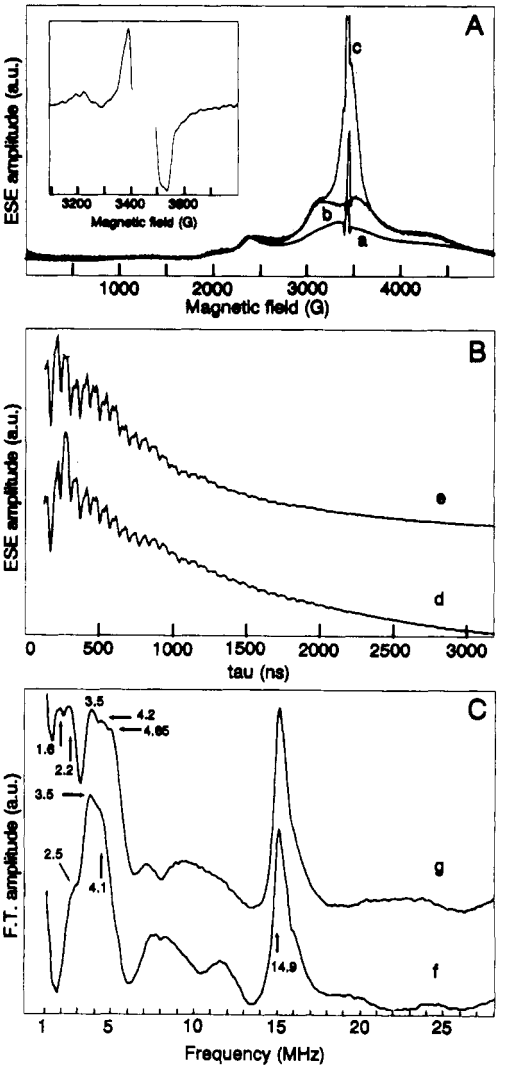

FIGURE 2: (Panel A) Amplitude of the electron spin echo as a function of the magnetic field for the following samples: trace a is obtained with PS II membranes treated with Tris; traces b and c are obtained with Ca^{2+}-depleted, EGTA-treated and polypeptide-reconstituted PS II membranes adapted in the dark, i.e., in the S_2 state (trace b), and after illumination at 0 °C, i.e., in the S_3 state (trace c). The inset shows the derivative with respect to the magnetic field of trace c *minus* trace b, with the artifact from the off-scale feature from the stable Tyr D• radical removed. (Panels B and C) Two-pulse ESEEM data (d, e) and corresponding Fourier transforms (f, g). Experimental conditions are the same as for Figure 1, except that the starting interpulse time τ was 96 ns for trace d. The spectra are obtained on samples made of Ca^{2+}-depleted, EGTA-treated and polypeptide-reconstituted PS II membranes from either ^{14}N (traces d, f) or ^{15}N (traces e, g) labeled material.

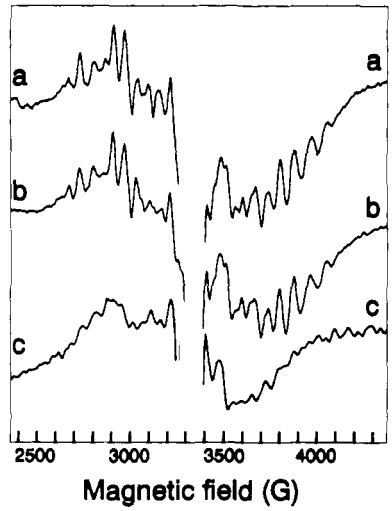

FIGURE 3: CW EPR spectra of Ca^{2+}-depleted/pyrophosphate-treated (spectrum a) and Ca^{2+}-depleted/EGTA-treated (spectrum b) PS II membranes. Instrument settings: temperature, 10 K; amplitude of field modulation, 20 G; microwave power, 20 mW; microwave frequency, 9.4 GHz. Spectrum c is the result of the numerical differentiation with respect to the magnetic field of trace b in panel A of Figure 2.

a sample that has been treated with Tris, thus destroying the Mn cluster. Since the EPR signal that can be detected in the CW mode for such a sample is assigned to the three g components (g_x = 1.49, g_y = 2.25, g_z = 2.95) of oxidized low-potential cytochrome b_{559} (Berthomieu et al., 1992b), the spectrum shown in Figure 2Aa was also assigned to this oxidized cytochrome b_{559}. Traces a and b in Figure 2A were scaled so that the amplitudes of the oxidized cytochrome b_{559} g_z feature exactly match. Comparison of the two spectra shows that there is a large increase in the EPR signal from ≈2600 to ≈4500 G. This, together with the known CW EPR properties of these samples, indicates that this central signal originates from the S_2 Mn signal from the OEC. After the dark-adapted sample treated with EGTA (giving rise to trace b) was advanced to the S_3 state, trace c in Figure 2A was obtained. Again the spectrum was scaled so that the g_z feature of oxidized cyt b_{559} matches those of the other two spectra. An intense signal is now visible in the $g \approx 2$ region that extends over roughly 200 G. The derivative of this spectrum with respect to magnetic field is shown in the inset of Figure 2A for comparison with conventional field-modulated spectra. The line width of this signal is close to 160 G, and we assign it to the same species that gives rise to the S_3 signal in the CW mode, namely, a radical species interacting with the Mn cluster. As mentioned above, the formation of this split S_3 signal corresponds to nearly complete advancement from the S_2 state to the S_3 state as judged by the CW EPR data (not shown). Furthermore, we have made a quantitative analysis of the echo-detected EPR signals by measuring the area under the traces b and c in Figure 2. The area between traces b and c (S_3; see below) compares well (ratio: 0.8) with the area between traces a and b (S_2). This clearly indicate that in the sample used the S_3 state was formed in nearly all the S_2 centers. Most interestingly, Figure 2A also shows that the broad signal that was assigned to the Mn signal in trace b is still present in trace c, i.e., after the S_3 state is formed. This indicates that the EPR signal originating from the Mn cluster can be detected in this mode both for the S_2 and S_3 states. This result substantiates the hypothesis made earlier (Boussac et al., 1990a) and recalled above about the origin of the S_3 signal and the lack of oxidation of the Mn cluster with $S = {}^1/_2$ during the S_2 to S_3 transition in the inhibited enzyme.

Two-pulse ESEEM traces obtained for the sample in the S_2 state of Ca^{2+}-depleted PS II membranes treated with EGTA are shown in Figure 2, panels B and C, together with the corresponding cosine FT. The samples were made from regular spinach leaves (i.e., 99.6% ^{14}N) (traces d and f) or from spinach grown from a ^{15}N source (traces e and g). Both samples exhibit the same stable modified Mn multiline signal from the S_2 state as measured by CW EPR, even when the signals were recorded with a field modulation amplitude of 12 G (not shown). This indicates that only relatively small nitrogen couplings to the Mn can be expected in this system. A similar situation was found for the oxygen-evolving PS II (Andréasson, 1989; DeRose et al., 1991). The two-pulse ESEEM of the ^{14}N sample measured at 3480 G shows two main features peaking at ≈3.5 and 14.9 MHz in the Fourier transform. These peaks resemble those shown for the control sample in the S_2 state (Figure 1C), but it is interesting to note that the lower frequency feature peaks at ≈3.5 MHz instead of ≈4.6 MHz in the control sample (Figure 1C). In the spectrum of the ^{15}N sample, the peak from weakly coupled protons is still present at 14.9 MHz. However, the pattern of peaks in the lower frequency region appears completely altered by the isotope substitution, indicating that these frequency components include couplings from nitrogen nuclei from protein residues. Close comparison of Figure 2C traces f and g shows the following: first, the broad feature that peaks at 3.5 MHz in the ^{14}N sample is still present in the ^{15}N sample but with a somewhat decreased amplitude (compare the relative amplitude with respect to the 14.9-MHz peak). In addition, the shoulder at 4.1 MHz in the ^{14}N sample is replaced by two features at 4.2 and 4.65 MHz upon isotope substitution; and second, a new peak with maxima at 1.6 and 2.2 MHz that is absent in the ^{14}N sample is clearly resolved in the ^{15}N spectrum (Figure 2Cg). That the broad peak at 3.5 MHz or at least part of it or parts of its features is still present after replacement of the protein ^{14}N atoms suggests that couplings from other sources than from protein ^{14}N nuclei have to be invoked to explain the origin of this peak. Experiments pertinent to the assignment of this peak are described below. The peaks at 1.6–2.2 MHz that are present in the ^{15}N sample but absent in the ^{14}N sample (Figure 2Cg) are assigned to couplings with one or more ^{15}N nuclei arising from protein residues.

It is of note that features almost identical to those displayed in the ESEEM spectra in Figure 2C were observed for a sample in which the treatment of EGTA was not followed by reconstitution with the 17- and 23-kDa extrinsic polypeptides (not shown). This indicates that the nitrogenous protein residues that are involved in the magnetic couplings shown in the ESEEM traces of Ca^{2+}-depleted, EGTA-treated PS II are not located on the 17- and 23-kD a extrinsic polypeptides. It also indicates that the presence or absence of these polypeptides does not affect the nitrogenous couplings that can be detected by ESEEM spectroscopy.

It has been proposed, on the basis of CW EPR results, that treatment of PS II with EGTA induces binding of one or more EGTA molecules to the Mn tetranuclear complex (Boussac et al., 1990b), thereby displacing native ligands to the Mn. Also, it is possible that the 3.5-MHz peak observed in the two-pulse FT-ESEEM of the EGTA-treated enzyme and which is present both in native and ^{15}N-substituted PS II may include contributions from ^{14}N from EGTA ligands. To address this question, PS II membranes were Ca^{2+}-depleted and treated with pyrophosphate instead of EGTA (see

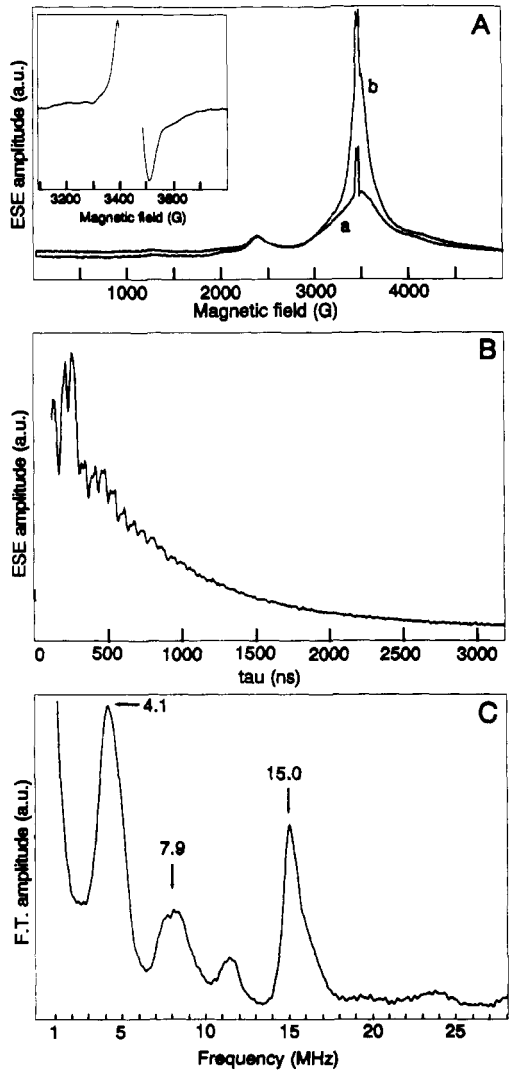

FIGURE 4: (Panel A) Echo-detected EPR signals of dark-adapted (trace a) and illuminated (trace b) Ca^{2+}-depleted, pyrophosphate-treated PS II membranes. The τ value used was 200 ns. The inset shows the derivative of trace b *minus* trace a with respect to the magnetic field. (Panel B) Two-pulse ESEEM trace of the dark-adapted sample (S_2 state). Magnetic field, 3480 G; starting τ, 112 ns; microwave frequency, 9.63 GHz; temperature, 3.9 K; time interval between pulse sets, 1.0 ms. (Panel C) Fourier transform of the data set shown in Panel B.

Materials and Methods). Figure 3a shows that after treatment of PS II membranes with sodium pyrophosphate, the multiline EPR signal from the S_2 state exhibits a modified pattern of hyperfine lines (with respect to that of the S_2 state of control PS II) that is virtually identical to that observed after treatment with EGTA (spectrum b). A period of illumination at 0 °C given to this sample followed by rapid freezing produced a broad EPR signal centered close to $g \approx 2$ and with a peak-to-peak width of ≈130 G, an EPR signal that is almost identical to that observed for the S_3 state of EGTA-treated material which has not been reconstituted with the extrinsic polypeptides (Boussac et al. 1990b) (not shown). These results suggest that the lesion in the OEC that is produced by the treatment with pyrophosphate is very similar to that caused by EGTA.

Figure 4A displays the echo-detected EPR signals from the S_2 and S_3 states in the Ca^{2+}-depleted, pyrophosphate-treated PS II. The spectra are similar to those observed for the Ca^{2+}-depleted, EGTA-treated PS II shown in Figure 2A. The inset in panel A shows the derivative of spectrum b and corresponds well to the S_3 signal with a line width of ≈130 G. Figure 4 panels B and C show the two-pulse ESEEM trace and the corresponding cosine-FT spectrum that were obtained at 3480 G for a sample treated with pyrophosphate. The spectrum exhibits two main peaks in the Fourier transform at 4.1 and 15.0 MHz. An additional feature with a lower amplitude is also resolved at ≈7.9 MHz and possibly also at ≈11 MHz (Figure 4C). This pattern of frequency lines is similar to that observed for the S_2 state of the control sample (Figure 1C) and the EGTA-treated sample (Figure 2C). Similarly, the 15.0-MHz peak in Figure 4C is ascribed to the resonance of weakly coupled protons. However, the following differences can be noted in the low-frequency region: (i) As is observed for the EGTA-treated sample, the low-frequency peak in the pyrophosphate sample appears at a frequency position (4.1 MHz) that is lower than in the control sample (4.5 MHz). (ii) The low-frequency peak in the FT-ESEEM of the pyrophosphate sample appears sharper than that in the EGTA sample, and the exact position of the line is different. In addition, this peak at 4.1 MHz lacks the substructure shown by the corresponding peaks in the other samples.

It is shown above that pyrophosphate and EGTA have very similar effects on the OEC. Thus it is reasonable to similarly assign the low-frequency peak at 4.1 MHz in the pyrophosphate-treated sample to nitrogen couplings. If this is the case, then since pyrophosphate cannot provide nitrogenous ligands to the Mn, the frequency peak at 4.1 MHz would be assigned to couplings with nitrogen nuclei from protein residues. In addition, since the low-frequency peak assigned to coupling to nitrogenous residues in the control PS II appeared at 4.6 MHz (Figure 1C), it is concluded that the Ca^{2+} depletion treatment and/or treatment with pyrophosphate perturbs the coupling characteristics of these ^{14}N-containing residues.

It is of note that a feature corresponding to the peak at 3.5 MHz, which may arise from ^{14}N from EGTA as suggested above, is not detectable in the pyrophosphate-treated sample. If this feature is absent from the spectrum and not obscured by overlapping signals, this observation may be taken as further support for the assignment of the 3.5-MHz peak to ^{14}N from EGTA.

In the following set of experiments, the Ca^{2+}-depleted samples were subjected to a period of illumination at 0 °C to allow advancement to the S_3 state. The experiment was performed for the samples treated with EGTA and made from either ^{14}N- or ^{15}N-labeled material, as well as for a third sample made from ^{14}N material treated with pyrophosphate. The S_2 to S_3 transition was monitored by CW EPR in these three samples by the disappearance of the S_2 multiline signal (see Figure 3a) and the formation of the split S_3 signal at $g \approx 2$. The two-pulse ESEEM signals for the three samples were then measured at 3480 G, i.e., at a magnetic field position where the contribution of the radical signal from the S_3 state dominates (see Figure 2A and 4A). Figure 5A shows the two-pulse ESEEM trace for the pyrophosphate-treated sample in the S_2 state (a) and in the S_3 state (b). Comparison of the two time domain data sets indicates that the ESEEM is not strongly affected by the illumination and that the changes in the ESEEM induced by the S_2 to S_3 transition are small. Figure 5Ac shows the difference time domain data S_3 minus S_2, and the Fourier transform of this difference is shown in Figure 5B (trace a). In addition, to remove from the ESEEM data the contribution of modulations that are unaffected by the S_2 to S_3 transition, the data set obtained for the S_3 state was divided by that of the S_2 state. The result is shown in Figure 5Ad, and the Fourier transform is shown in Figure 5Bb. In spite of the increase in the noise level that results

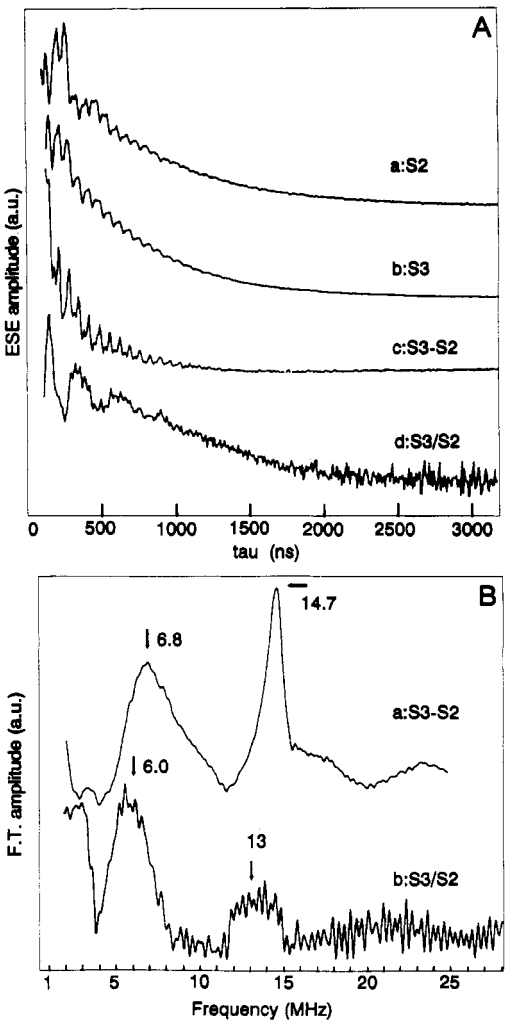

FIGURE 5: (Panel A) Two-pulse ESEEM traces of Ca^{2+}-depleted and pyrophosphate-treated PS II membranes: trace a is from the dark-adapted sample (S_2 state); trace b is after illumination at 0 °C (S_3 state); trace c is trace b *minus* trace a; and trace d is trace b *divided* by trace a. Magnetic field, 3480 G; microwave frequency, 9.63 GHz; temperature, 4.2 K; starting τ, 112 ns; time interval between successive pulse sets, 1.0 ms. (Panel B) Traces a and b are the Fourier transform spectra of traces c and d in panel A, respectively.

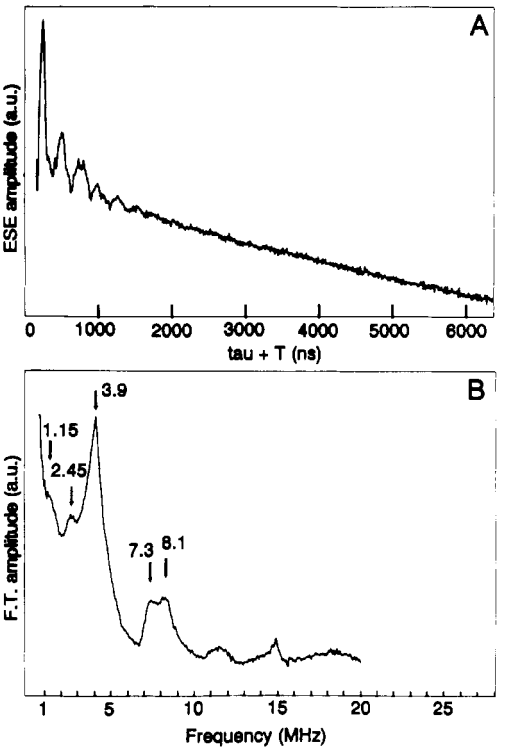

FIGURE 6: (Panel A) Three-pulse ESEEM trace of dark-adapted PS II membranes that are Ca^{2+}-depleted and treated with pyrophosphate. The data set was recorded at a magnetic field of 3480 G, a microwave frequency of 9.63 GHz, and a τ value of 136 ns. The interpulse time T was incremented from 40 to 6432 ns in 8-ns steps. Repetition time between successive pulse shots is 1.0 ms. (Panel B) Fourier transform of the data set shown in panel A.

from the ratioing procedure, a large peak is resolved at ≈6–7 MHz, a peak that is also present in the spectrum of the difference data (trace a), with possibly another feature centered at ≈13.3 MHz. In addition, the positive feature at ≈2–3 MHz may also represent a real component of the frequency spectrum. These peaks appear as positive features in the data obtained as a ratio, indicating that they correspond to couplings that are present in the S_3 state, but not in the S_2 state. There is no negative feature in the Fourier transform, indicating that the proton and nitrogen couplings to the Mn present in the S_2 state are still present in the S_3 state. The features at 6–7 MHz and ≈13 MHz were also observed for the ratio data obtained at other magnetic field positions *throughout* the S_3 signal (not shown). However, the ratio ESEEM data taken at magnetic field positions *below* ≈3350 G or *above* ≈3500 G, i.e., *outside* the S_3 signal, do not show these extra features (data not shown). This result indicates that these features at 6–7 MHz (and possibly 13 MHz) correspond to couplings that are associated with the species that gives rise to the S_3 split EPR signal.

The signal-to-noise ratio of the ratio signal obtained for the samples made with EGTA-treated PS II membranes was poorer than that obtained for the pyrophosphate-treated sample. We were thus unable to determine if similar features at 6–7 MHz and ≈13 MHz were also present in the FT spectra of EGTA-treated samples prepared from ^{15}N- or ^{14}N-labeled PS II membranes. One explanation for this behavior could lie in the increased complexity of the ESEEM for the EGTA-treated material compared with the pyrophosphate-treated membranes (compare Figure 2C with Figure 4C).

Three-pulse ESEEM data sets were also collected, for each of the samples mentioned above. For all the samples except the sample with pyrophosphate-treated PS II, the modulation was extremely shallow, leading to an FT spectrum with much less resolution than the corresponding two-pulse FT spectra. This was observed for a number of different τ values. In principle, analysis of the frequencies in the FT spectrum of the three-pulse ESEEM is less complicated because the sum and difference frequencies that occur in the two-pulse spectrum are now absent. Unfortunately, this was not possible in this study, due to the low-resolution of the three-pulse FT-ESEEM spectra that were obtained. The one exception is the pyrophosphate-treated sample in the S_2 state. Figure 6 shows the three-pulse ESEEM (panel A) together with the corresponding cosine-Fourier transform (panel B) obtained at 3480 G for such a sample. The τ value (τ = 136 ns) was chosen in order to suppress the modulation at 15.0 MHz due to weakly coupled protons in the corresponding two-pulse ESEEM (see Figure 4C). A rather well-defined modulation is present in the time domain data set that corresponds to the intense narrow peak at 3.9 MHz in the Fourier transform. Another component around 7–8 MHz is also resolved together with other minor components at ≈1.15, 2.45, and 11.1 MHz. These peaks are very close to those shown in the Fourier transform of the corresponding two-pulse ESEEM, indicating that none of them is a sum or difference peak and that they are true

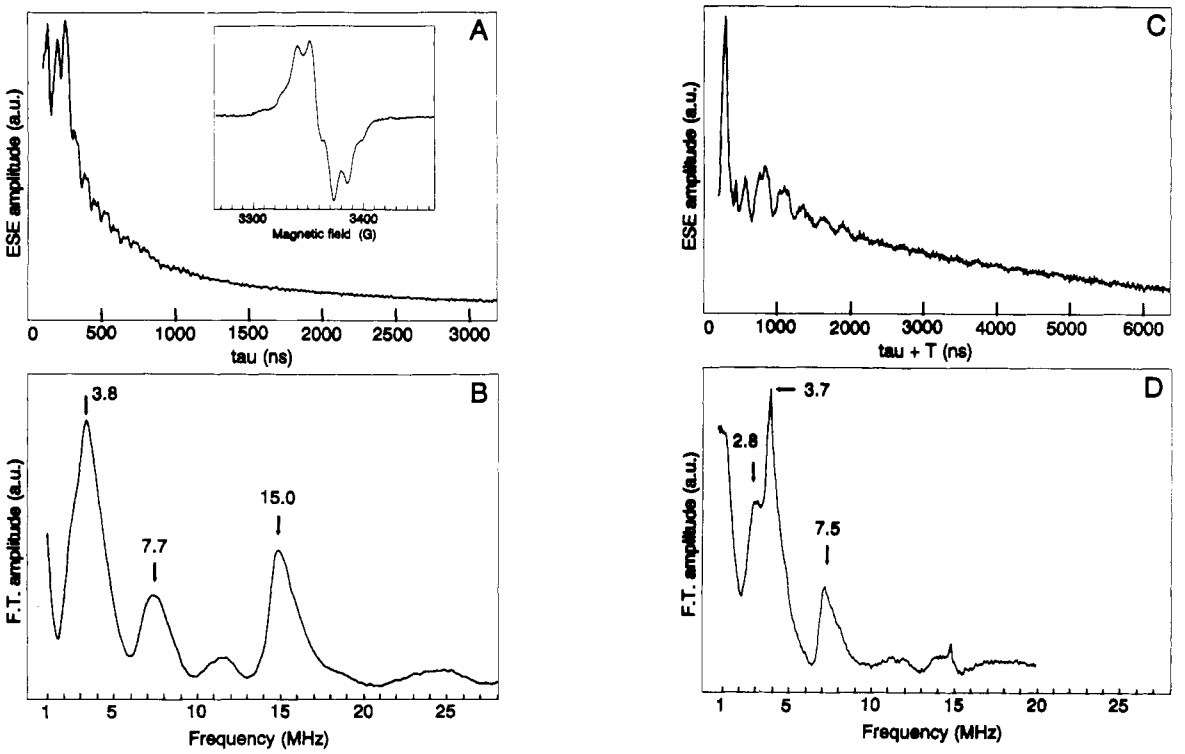

FIGURE 7: (Panels A and B) Two-pulse ESEEM data (A) and Fourier transform (B) of a sample made of a frozen solution of UV-irradiated 4(5)-CH_3-imidazole. Magnetic field, 3472 G; microwave frequency, 9.72 GHz; temperature, 3.9 K; starting τ value, 104 ns. The inset shows the CW EPR spectrum recorded on the same sample with the following experimental conditions: T = 20 K; modulation amplitude, 2.8 G; power, 63 μW; frequency, 9.4 GHz. The spectrum is centered at g = 2.0038. (Panels C and D) Three-pulse ESEEM data (C) and Fourier transform (D) obtained on the same sample. τ = 136 ns; starting T value, 32 ns. Other experimental conditions: Magnetic field, 3472 G; microwave frequency, 9.72 GHz; shot repetition time, 2.1 ms.

frequency components of nitrogen couplings.

To understand the nature of the radical species that gives rise to the S_3 split EPR signal and to understand the origin of the nitrogen couplings that are detected in the ESEEM in the S_3 state, we have compared the ESEEM data shown above with the ESEEM data that could be obtained for a number of organic radicals produced by UV irradiation of amino acids which might be functionally involved in the OEC. The radicals that were studied are Tyr•, Trp•, Phe•, Im•, and 4(5)-CH_3-Im•. In addition, the effect of isotopic substitution ($^{14}N/^{15}N$) was also studied for Im•. The two- or three-pulse FT-ESEEM spectra obtained at 3460 G for Tyr•, Trp•, and Phe• merely revealed the free proton frequency at 14.9 MHz. No other frequency component was evident in our measurements, except for Tyr•, where a small signal at ≈1.5 MHz was resolved, probably arising from coupling of the electron spin with one of the β-methylene protons (Evelo et al., 1989; Barry et al., 1990). Only the spectra obtained with the imidazole moiety showed additional components in the low-frequency range. In addition, the ESEEM patterns were different for ^{14}N- and ^{15}N-labeled amino acids, indicating that the radicals that are formed by the UV irradiation do arise from amino acid radicals and are not associated with the solvent (Boussac et al., 1992a). Figure 7 panels A and B show the two-pulse ESEEM data and Fourier transform obtained for the 4(5)-CH_3-Im• radical. The two-pulse spectrum shows two main peaks at 3.8 and 15.0 MHz, together with smaller features at 7.7 and 11.7 MHz. Surprisingly, this pattern is strikingly similar to that obtained for the pyrophosphate-treated enzyme in the S_2 state and shown in Figure 4C. It is already argued above that the low-frequency pattern in the pyrophosphate-treated enzyme corresponds to nitrogen hyperfine couplings with the electron spin on the Mn. By contrast, the frequency components resolved in the Im• spectrum (Figure 7B) originate from couplings between ^{14}N from the imidazole ring and the electronic spin on the imidazole itself. The remarkable similarities of the two spectra (which are also seen in the three-pulse spectra; compare Figure 7D with Figure 6B), make it tempting to suggest that the coupling pattern seen for the Mn in the pyrophosphate-treated sample in the S_2 state in some way reflects nitrogen couplings from an imidazole moiety.

DISCUSSION

We have detected the EPR signals arising from the Mn complex in Ca^{2+}-depleted PS II both in the S_2 and the S_3 states by echo-detected EPR: upon formation of the split EPR signal in the S_3 state, the broad EPR signal from the S_2 state does not disappear. This is strong evidence that the oxidation state of the Mn complex is the same in the S_2 and the S_3 states. This result also supports our previous model of the Ca^{2+}-depleted enzyme in which we proposed an amino acid residue as the electron donor in the S_2 to S_3 transition, with no oxidation of the Mn tetranuclear cluster (Boussac et al., 1990a). Regarding the CW EPR spectroscopy results, presumably the EPR multiline signal of the Ca^{2+}-depleted enzyme is broadened in the S_3 state so that it becomes undetectable in the conventional field modulated mode. However, when the absorption is directly measured, as is the case when the amplitude of the two-pulse echo is measured as a function of the magnetic field, the EPR signal can be detected. This advantage of echo-detected EPR over CW EPR has already been pointed out [see, e.g., Britt et al. (1992)].

The two-pulse ESEEM data are reported for the EPR multiline signal in the S_2 state of oxygen-evolving PS II. The results are similar to those reported under similar conditions by Britt et al. (1989) and by DeRose et al. (1991). These authors interpreted a low-frequency peak at ≈4.5 MHz as

arising from hyperfine couplings with ^{14}N either directly ligated to the Mn cluster or through a hydrogen bond (DeRose et al., 1991). However the spectrum reported in the present study (Figure 1C) shows additional features in the lower frequency region compared to the earlier reports: the ^{14}N peak at low frequency has resolved features at 2.3, 3.6, and 4.6 MHz. It is of note that this ESEEM pattern was obtained at 3480 G, a magnetic field position where the contribution of the S_2 Mn signal dominates but also where other paramagnetic species may also contribute. That these extra features in Figure 1C may arise from the EPR signal of oxidized cytochrome b_{559} can probably be eliminated because the same frequency pattern was found after the ESEEM recorded for the background signal in the S_1 state that originates from oxidized cytochrome b_{559} was subtracted (compare Figure 1C, traces e and f). The echo-detected EPR spectrum displayed in Fig 1A shows a signal at $g \approx 1.9$ that may originate from the semiquinone Fe^{2+} acceptor complex of PS II that is reduced by the illumination procedure. Although some contribution from this complex in the ESEEM shown in Figure 1B,C cannot be completely ruled out, any important distortion that would bias the conclusions made here seems unlikely for the following reasons: (i) a low-frequency peak at the same frequency position (with possible resolution) was observed by other groups also (Britt et al., 1989: DeRose et al., 1991); (ii) a similar low-frequency pattern with three resolved peaks was observed in the FT ESEEM measured at other frequency positions where little contribution from the acceptor side signals can be expected (not shown); and (iii) a similar pattern of peaks is observed for the EGTA-treated sample, where the quinone–iron complex is oxidized in the dark-adapted S_2 state.

While a number of detailed pulsed EPR studies on Cu^{2+}-containing enzymes have been published (McCracken et al., 1992 and references therein), only a few ESEEM data have been reported for enzymes containing manganese. However, recent results obtained by McCracken et al. (1992) on several Cu^{2+}-containing amine oxidases seem relevant to those reported here: similar to the low-frequency feature observed for the ESEEM of the Mn S_2 signal, a single low-frequency feature at $\approx$3.3 MHz attributable to ^{14}N coupling has been found in the ESEEM spectra of the substrate-derived radical of *Arthrobacter* P1 methylamine oxidase and of porcine kidney amine oxidase (McCracken et al., 1992). The ESEEM spectra could be successfully simulated with ^{14}N couplings with large isotropic and anisotropic hyperfine interactions (McCracken et al., 1992). Judging from the similarity of the ESEEM data reported here for the S_2 state of the OEC and those reported for the amine oxidases (McCracken et al., 1992), it is quite possible to use the same theoretical framework to explain the modulations arising from the ^{14}N couplings to the Mn. Thus, large anisotropic hyperfine interactions with ^{14}N nuclei would be responsible for the ESEEM detected here and the splitting of the $\approx$4 MHz peak would indicate coupling to three different classes of ^{14}N nuclei with the Mn complex in the S_2 state. In addition, large anisotropic hyperfine interactions are unlikely to be observed with distant ^{14}N. Thus, this model favors also a situation in which the nitrogen atoms are either coordinated to the Mn or interact through hydrogen bonds, as originally proposed by DeRose et al. (1991).

Treatment of Ca^{2+}-depleted PS II membranes with EGTA is accompanied by the appearance of an S_2 state with an EPR multiline signal that displays a modified pattern of hyperfine lines (Boussac et al., 1989), compared with that displayed by the untreated PS II. The ESEEM frequencies around 4 MHz that are attributed to ^{14}N couplings are also different as judged by the different ESEEM patterns (compare Figure 2C with Figure 1C). It is suggested (see below) that the 3.5-MHz component in the data of the Ca^{2+}-depleted enzyme is at least partly attributable to coupling with ^{14}N from EGTA. However, the narrowing of the low-frequency peak in Ca^{2+}-depleted material and the shifts observed for the lines both indicate a modification of the peptide ^{14}N couplings in the Ca^{2+}-depleted enzyme. This is strong evidence for a structural rearrangement very close to the Mn cluster induced by the Ca^{2+} depletion procedure and/or EGTA treatment. In addition, as mentioned above, the ESEEM of ^{15}N-substituted oxygen evolving PS II in the S_2 state has been reported by DeRose et al. (1991), and the corresponding FT did not show any frequency attributable to ^{15}N couplings.[2] In the present study, ESEEM data on ^{15}N-substituted Ca^{2+}-depleted and EGTA-treated PS II are reported, with a number of frequencies originating from ^{15}N interactions (Figure 2C). While the origin of these differences in the nitrogenous couplings between the two samples is not known, it itself shows again a significant modification of the structure around the Mn cluster induced by the Ca^{2+} depletion and/or the EGTA treatment.

The presence or absence of the 24- and 17- kDa extrinsic polypeptides that are associated with the oxygen-evolving complex does not influence the values of the ^{14}N couplings to the Mn cluster in Ca^{2+}-depleted, EGTA-treated PS II. This indicates that the nitrogen-containing residues responsible for the observed ^{14}N couplings are not located on these polypeptides. Nor does the absence of these polypeptides influence these superhyperfine couplings.

When the Ca^{2+} depletion treatment is followed by addition of pyrophosphate instead of EGTA, the two-pulse ESEEM pattern is significantly altered. The low-frequency peak is much narrower at 4.1 MHz, and the features that were resolved on top of the peak in the EGTA sample are now absent. It is demonstrated above that the CW EPR results are identical in the two samples, indicating a similar lesion by EGTA and pyrophosphate following the Ca^{2+} depletion treatment. The difference in the ESEEM patterns is suggested above to arise from superhyperfine couplings due to EGTA. Alternatively, coupling to ^{31}P from the pyrophosphate may contribute to the differences in the ESEEM data. Another significant difference between the pyrophosphate- and the EGTA-treated samples is that the three-pulse ESEEM data showed a very deep modulation (from ^{14}N) for the former (see Figure 6), while only a very shallow modulation (from ^{14}N) was observed for the latter (not shown). This situation is not abnormal *a priori* since modulation depths are critically dependent on nuclear-state mixing and other examples can be found in the literature [see McCracken et al. (1992)]. However, the differences observed here strongly suggest that the modulations observed in the two-pulse ESEEM of the EGTA and the pyrophosphate samples have different origins. We propose that EGTA binds to the Mn tetranuclear cluster and that the nitrogenous ligands give rise to the coupling observed at 3.5 MHz in the ESEEM.

Couplings from ^{14}N nuclei are also detected in the ESEEM data recorded for the S_3 state of the pyrophosphate-treated

[2] It could be argued that DeRose et al. (1991) reported S_2 *minus* S_1 difference spectra and that the spectra shown here could be contaminated by modulations from species present in the dark, i.e., oxidized cytochrome b_{559}. This seems unlikely because the pattern of frequencies reported for the S_2 state is virtually identical to that of the subtracted data set S_2 *minus* S_1 (see Figure 1C). In addition, the frequency pattern reported here is very different from that reported for the oxidized cytochrome b_{559} (two large peaks at $\approx$4 and $\approx$7 MHz) by DeRose et al. (1991).

enzyme: data were obtained at several magnetic field positions throughout the S_2 Mn signal. The data for the S_2 and for the S_3 state, both recorded outside the split S_3 signal, are virtually identical, confirming that the couplings for the Mn cluster are unchanged in the S_2 to S_3 transition in the inhibited enzyme. However, the S_3/S_2 ratio data obtained at magnetic field positions throughout the split S_3 signal show two positive features in the Fourier transform at 6.0 and 13.3 MHz, with possibly another peak at lower frequency (Figure 5B). In addition, as was observed at other magnetic field positions, the ratio data do not show any negative feature that would correspond to couplings that disappear during the S_2 to S_3 transition. This indicates that the ^{14}N couplings present in the S_2 state are the same in the S_3 state. The origin of the positive features resolved at 6–7 MHz and ≈13 MHz in the S_3/S_2 ratio data is much less clear. Since these were best resolved in the pyrophosphate-treated sample, it is possible that they correspond to superhyperfine couplings with ^{31}P; indeed, couplings similar to those reported here have been detected in Mn(II)-pyrophosphatase and attributed to dipolar couplings of phosphoryl ligands with enzyme bound Mn(II) (Banerjee et al., 1987). However, at present it seems equally likely that these features also originate from ^{14}N couplings.

The $S = {}^1/_2$ ground spin state from the organic radical that is formed in the S_3 state interacts with the paramagnetic Mn cluster and gives rise to the split S_3 EPR signal observed around $g \approx 2$. From the magnitude of the dipolar broadening derived from the computer simulation of the S_3 split signal (40 G; Boussac et al., 1990a), a lower limit of $R \approx 6$ Å can be estimated for the distance separating the radical and the Mn cluster (J. L. Zimmermann, unpublished).[3] The radical has been proposed to be a histidine residue on the basis of its absorption spectrum in the UV (Boussac et al., 1990a). It seems unlikely that this 6 Å or more-distant histidine also gives rise to the nitrogen modulations observed in the S_2 state and reported here, as these would be expected to be strongly modified upon oxidation of the histidine. As shown above, the modulations attributed to couplings with ^{14}N are conserved during the S_2 to S_3 transition. We propose that nitrogens from amino acids other than the putative redox active histidine are located close to the Mn cluster and are responsible for these couplings. As mentioned above, the amplitude of these couplings are indicative of either directly coordinated nitrogens or nitrogens which are coordinated through hydrogen bonds.

The two- and three-pulse ESEEM spectra are reported for the 4(5)-CH_3-Im$^\bullet$ radical. The spectra show a pattern of peaks in the low-frequency region that is attributed to ^{14}N lines and is almost identical to that observed for the pyrophosphate-treated PS II in the S_2 state. Of particular note is the depth of the modulation that transforms into the quite narrow peak at ≈4 MHz, which is present in both spectra. Rather unexpectedly, the nitrogen hyperfine couplings in the imidazole radical are quite small. However, relatively small nitrogen hyperfine coupling constants are also observed in the CW EPR spectra [Boussac et al., 1992a; see also Rhodes (1990)]. The strong similarity of the ESEEM spectra of the imidazole radical with those of the S_2 state of the Ca^{2+}-depleted, pyrophosphate-treated PS II may indicate that the electron spin density on the nitrogen atoms in the imidazole radical is comparable to that found in the Mn center of the OEC. In the latter, the electron spin density on the nearby nitrogens is expected to be small because the large value of the ^{55}Mn hyperfine coupling constants indicates a large electron spin density on the Mn atoms themselves. In addition, the strong similarity of the two ESEEM patterns may argue for (a) histidine ligand(s) to the Mn cluster.

The ESEEM spectra taken on the imidazole radical were obtained as a reference for comparison with the ESEEM from the split S_3 radical. The results were rather ambiguous for several reasons. First, the ESEEM patterns for the imidazole radical turned out to be surprisingly like that from the Mn signal in the S_2 state. Secondly, the ESEEM for the S_3 state was only obtainable by taking the ratio of the S_2 and S_3 spectra, and since the expected ESEEM features for the imidazole radical are in the same region as the features for the Mn in the S_2 state, they might be canceled out in the S_3/S_2 data set. And thirdly, the ESEEM for the S_3 state had only a rather poor signal-to-noise ratio and was only obtainable for the pyrophosphate-treated sample. As a result, features at low frequency were difficult to resolve. We conclude that the data neither confirm nor eliminate "histidine" as the origin of the split S_3 signal.[4]

[3] An upper limit of ≈12 Å can also be computed from the value of the exchange coupling constant.

[4] While this paper was in preparation, results from pulsed EPR on Ca^{2+}-depleted PS II were presented at the 9th International Congress on Photosynthesis in Nagoya, Japan. The echo-detected EPR results presented by R. D. Britt (Gilchrist et al., 1992) appear to differ significantly from ours on a number of points, and it is presently difficult to understand the origin of the discrepancies.

ACKNOWLEDGMENT

We thank R. David Britt for providing a preprint of his paper (Gilchrist et al., 1992). J.L.Z. thanks John McCracken for providing the source code of his data analysis routine as well as for extremely useful discussions regarding the data reconstruction technique.

REFERENCES

Andréasson, L.-E. (1989) *Biochim. Biophys. Acta 973*, 645–467.

Andréasson, L.-E. & Lindberg, K. (1992) *Biochim. Biophys. Acta 1100*, 177–183.

Banerjee, A., McCracken, J. L., Peisach, J., & Cooperman, B. S. (1987) *Fed. Proc. 46*, 2042.

Baumgarten, M., Philo, J. S., & Dismukes, G. C. (1990) *Biochemistry 29*, 10814–10822.

Barry, B. A., El-Deeb, M. K., Sandusky, P. O., & Babcock, G. T. (1990) *J. Biol. Chem. 265*, 20139–20143.

Beck, W. F., dePaula, J. C., & Brudvig, G. W. (1986) *J. Am. Chem. Soc. 108*, 4018–4022.

Berthold, D. A., Babcock, G. T., & Yocum, C. F. (1981) *FEBS Lett. 61*, 231–234.

Berthomieu, C., Nabedryk, E., Breton, J., & Boussac, A. (1992a) in *Research in Photosynthesis* (Murata, N., Ed.) Vol. II, pp 53–56, Kluwer Academic Publishers, Dordrecht, The Netherlands.

Berthomieu, C. Boussac, A., Mäntele, W., Breton, J., & Nabedryk, E. (1992b) *Biochemistry 31*, 11460–11471.

Bonvoisin, J., Blondin, G., Girerd, J.-J., & Zimmermann, J.-L. (1992) *Biophys. J. 61*, 1076–1086.

Boussac, A., & Rutherford, A. W. (1988) *Biochemistry 27*, 3476–3483.

Boussac, A., Zimmermann, J.-L., & Rutherford, A. W. (1989) *Biochemistry 28*, 8984–8989.

Boussac, A., Zimmermann, J.-L., Rutherford, A. W., & Lavergne, J. (1990a) *Nature 347*, 303–306.

Boussac, A., Zimmermann, J.-L., & Rutherford, A. W. (1990b) *FEBS Lett. 277*, 69–74.

Boussac, A., Zimmermann, J.-L. & Rutherford, A. W. (1992a) in *Research in Photosynthesis* (Murata, N., Ed.) Vol. II, pp 235–238, Kluwer Academic Publishers, Dordrecht, The Netherlands.

Boussac, A., Sétif, P., & Rutherford, A. W. (1992b) *Biochemistry 31*, 1224–1234.

Britt, R. D. (1988) Ph.D. Thesis, University of California, Berkeley, CA.

Britt, R. D., Zimmermann, J.-L., Sauer, K., & Klein, M. P. (1989) *J. Am. Chem. Soc. 111*, 3522–3532.

Britt, R. D., Lorigan, G. A., Sauer, K., Klein, M. P., & Zimmermann, J.-L. (1992) *Biochim. Biophys. Acta 1140*, 95–101.

Debus, R. J. (1992) *Biochim. Biophys. Acta 1102*, 269–352.

DeRose, V. J., Yachandra, V. K., McDermott, A. E., Britt, R. D., Sauer, K., & Klein, M. P. (1991) *Biochemistry 30*, 1335–1341.

Dismukes, G. C., & Siderer, Y. (1981) *Proc. Natl. Acad. Sci. U.S.A. 78*, 274–278.

Dismukes, G. C., Tang, X.-S., Khangulov, S. V., Sivaraja, M., Pessiki, P., & Barynin, V. V. (1992) in *Research in Photosynthesis* (Murata, N., Ed.) Vol. II, pp 257–264, Kluwer Academic Publishers, Dordrecht, The Netherlands.

Evelo, R. G., Hoff, A. J., Dikanov, S. A., & Tyryshkin, A. M. (1989) *Chem. Phys. Lett. 161*, 479–484.

Fauth, J.-M., Schweiger, A., Braunschweiler, L., Forrer, J., & Ernst, R. (1986) *J. Magn. Reson. 66*, 64–75.

Gilchrist, M. L., Lorigan, G. A., & Britt, R. D. (1992) in *Research in Photosynthesis* (Murata, N., Ed.) Vol. II, pp 317–320, Kluwer Academic Publishers, Dordrecht, The Netherlands.

Guiles, R. D., Zimmermann, J.-L., McDermott, A. E., Yachandra, V. K., Cole, J. L., Dexheimer, S. L., Britt, R. D., Wieghardt, K., Bossek, U., Sauer, K., & Klein, M. P. (1990) *Biochemistry 29*, 471–485.

Hallahan, B. J., Nugent, J. H. A, Warden, J. T., & Evans, M. C. W. (1992) *Biochemistry 31*, 4562–4573.

Kevan, L. (1990) in *Modern Pulsed and Continuous Wave Electron Spin Resonance* (Kevan, L., & Bowman, M. K., Eds) pp 231–266, Wiley Interscience, New York.

Krieger, A. (1992) Ph.D. Thesis, University of Düsseldorf, Düsseldorf, Germany.

McCracken, J., Peisach, J., Cote, C. E., McGuirl, M. A., & Dooley, D. M. (1992) *J. Am. Chem. Soc. 114*, 3715–3720.

McLachlan, D. J., Nugent, J. H. A., Strange, R. W., Hasnain, S. S., & Evans, M. C. W. (1992) *Proc. Int. Congr. Photosynth., 9th*, Nagoya, Japan.

Mims, W. B. (1984) *J. Magn. Reson. 59*, 291–306.

Mims, W. B., Davis, J. L., & Peisach, J. (1984) *Biophys. J. 45*, 755–766.

Ono, T.-A. & Inoue, Y. (1990) *Biochim. Biophys. Acta 1020*, 269–277.

Ono, T.-A., Noguchi, T., Inoue, Y., Kusunoki, M., Matsushita, T., & Oyanagi, H. (1992) *Science 258*, 1335–1337.

Rhodes, C. J. (1990) *J. Chem. Phys., Perkin Trans. 2*, 725–727.

Rutherford, A. W., & Zimmermann, J.-L. (1984) *Biochim. Biophys. Acta 767*, 168–175.

Rutherford, A. W., Boussac, A., & Zimmermann, J.-L. (1991) *New J. Chem. 15*, 491–500.

Rutherford, A. W., Zimmermann, J.-L., & Boussac, A. (1992) in *The Photosystems: Structure, Function and Molecular Biology* (Barber, J., Ed.) Chapter 5, pp 179–229, Elsevier Science Publishers, New York.

Sivaraja, M., Tso, J., & Dismukes, G. C. (1989) *Biochemistry 28*, 9459–9464.

Thorp, H. H., & Brudvig, G. W. (1991) *New J. Chem. 15*, 479–490.

Yachandra, V. K., Guiles, R. D., McDermott, A. E., Cole, J. L., Britt, R. D., Dexheimer, S. L., Sauer, K., & Klein, M. P. (1987) *Biochemistry 26*, 5974–5981.